Communications on Applied Nonlinear Analysis
ISSN: 1074-133X
Vol 31 No. 1s (2024)

Mathematical Modelling for Failure Analysis of Composite Drive Shaft Using Modal Flexibility and Curvature Method

Mr. Rakesh Raushan[1]*, Dr. K.K. Dhande[2], Dr. N.I. Jamadar[3]

[1]Dr. D Y Patil Institute of Technology, Pimpri, Pune, India

[2]Professor, Dr. D Y Patil Institute of Technology, Pimpri, Pune, India

[3]Associate professor, Dr. D Y Patil Institute of Technology, Pimpri, Pune, India

*Email- rakesh.raushan@dypvp.edu.in

Article History:

Received: *26-01-2024*

Revised: *24-03-2024*

Accepted: *16-04-2024*

Abstract:

Early damage identification in composite structures has attracted a lot of attention in post-failure examinations in recent years. In the research, torsional fatigue test of composite drive shafts has been done and numerical methodologies have been employed for the validation for premature failure using modal flexibility and modal curvature methods. Initially, the eigenvalue and eigenvectors of healthy and fractured drive shafts are evaluated using a numerical model and verified by fatigue experimental approach. Flexibility variance and the absolute curvature difference between the drive shafts that are fractured and those that are healthy are evaluated after mass normalization. Variations in absolute modal curvatures and variations in local flexibilities that are utilized to identify the existence, location, and severity of a drive shaft fracture. The position and severity of the fracture are predicted more precisely by the modal curvature approach than by the modal flexibility approach.

Keywords: Damage detection, Modal flexibility, Modal curvature, Numerical, healthy and fractured drive shafts.

List of Symbols

M Mass Matrix of intact drive shaft

M* Mass matrix of fractured drive shaft

K Stiffness matrix of intact drive shaft

K* Stiffness matrix of fractured drive shaft

l Equal length of drive shaft of all three parts

K_A Global Stiffness Matrix of intact drive shaft

K_A* Global Stiffness Matrix of fractured drive shaft

M Global Mass Matrix of healthy drive shaft

M* Global Mass matrix of damaged drive shaft

λ Eigen Values modal displacement of node j at mode i $\psi(j)_i$ nodal displacement of i^{th} mode of node j

U Modal displacements

$[F]_{hx}$ Flexibility coefficient matrix of intact drive shaft at distance x from fixed end

$[F]_{dx}$ Flexibility coefficient matrix of fractured drive shaft at distance x from fixed end

U_h Mass normalized Modal vector of intact drive shaft

U_d Mass Normalized modal vector of fractured drive shaft

Δ [F] Change in Flexibility Matrix

Mx At a distance x from the fixed end, the intact drive shaft's bending moment

M_x^* At a distance x from the fixed end, the fractured drive shaft's bending moment

Kx Curvature of healthy drive shaft at distance x from fixed end

K_x^* Curvature of damaged drive shaft at distance x from fixed end

Δ [K] Curvature difference

U_{h1}, U_{h2}, U_{h3} Eigen vectors of intact drive shaft after mass normalization for first three modes respectively.

U_{d1}, U_{d2}, U_{d3} Eigen vectors of fractured drive shaft after mass normalization for first three modes respectively.

K_{h1}, K_{h2}, K_{h3} Modal curvatures of intact drive shaft for first three modes respectively.

K_{d1}, K_{d2}, K_{d3} Modal curvatures of fractured drive shaft for first three modes respectively.

$\Delta[K]_1, \Delta[K]_2, \Delta[K]_3$ Difference in magnitude of modal curvature for the first three mode shapes respectively

1. Introduction

Due to its excellent specific strength, low weight, and corrosion resistance, composite materials are now widely employed in a variety of automobile parts. However, the biggest disadvantage of these materials is the complexity of their failure mechanism as compared to conventional materials. Low fatigue cycle failure in composite structures is caused by flaws that arise during manufacture or when the structure is in use. These flaws include delimitation, the coalescence of micro cracks, and other types of damage that occur as a result of cyclic loading. This defect can propagate and eventually lead to catastrophic failure if not detected and repaired on time. A difficult job is the gradual appraisal of such damages at intermediate stages.

N.I. Jamadar et.al [1,2] used the modal flexibility and modal curvature techniques were proposed numerically, exhibited accurate results in detecting the damages of healthy and damaged elements when used to locate damage in composite Mono Leaf Springs. In the next literature author identified the crack location in cracked spring with the help of Modal strain energy method.Dawari.et.al [3] employed modal flexibility and modal curvature techniques to determine crack in a reinforced beam and demonstrated that damage located at the highest absolute values of modal curvature difference. Pandey and Biswas [4] introduced the modal flexibility approach to locate damage in flanged beams. They found that results are more appropriate in lower frequency mode as compared to higher-frequency modes. Reynders et al [5] used the flexibility approach to determine the local stiffness to find the damage in a reinforced beam and where it is located. Yang et al. [6] employed a scale wave number domain filtering approach and discrete Fourier transform-based modal curvature to examine the damage in a carbon-reinforced polymer beam with and without a fracture. Yuen [7] provided research on how variations in eigenvalue and eigenvector may be used to determine the location of damage as well as the extent of the harm. V.S. Bhajantri et al. [8] developed high-strength carbon fibres reinforced with epoxy drive shaft and simulation and analysis were performed. Dai Gil Lee et

al. [9] utilized press-fitting to boost reliability and to save production costs as compared to alternative joining methods such adhesively bonded, bolted, riveted, and welded connections. A one-piece automobile hybrid aluminium/composite drive shaft was used in place of typical two-piece steel drive shafts by the researcher using this technique. Lestari and Qiao [10] performed an experimental investigation using a piezoelectric sensor and the form of the curvature model to determine the damage site in a sandwich beam made of fibre-reinforced polymer (E-glass). They observed that in lower modes curvatures more accuracy and precision is obtained for locating the fracture than in higher modes. Bauer [11] investigated the vibration behaviour of a rotating element with uniform spin along the length by treating it as a beam for all possible boundary conditions of the beam. In this paper, it is observed that, in all the cases with the variation in spin frequency, natural frequencies vary linearly. Kataev et.al [12] computed the stress and strain of the hollow polymer composite shafts. It was found that equal magnitude of tensile and compressive stresses act at an angle of 45^0 to the axis of the shaft which leads to the loss of stability of the shaft wall. Finally, it was observed that with the appropriate thickness and proper alignment, the instability can be minimized. C. Elanchezhian et.al [13] presented the Modelling and analysis comparison for conventional and composite drives shafts. Finally, they tested the composite drive shaft for strength and efficiency purposes. P. Satheeshkumar Reddy et al [14] explored Static, free vibration and torsional buckling analysis for composite and conventional drive shafts and researchers suggested the suitability of the composite drive shaft as compared to existing steel drive shafts in automobile industries. Banerjee et al. [15-17] used the Wittrick-William algorithm in their numerous research papers to calculate frequencies. The researcher developed the dynamical stiffness matrix of a centrifugally stiffened Timoshenko beam in one of his publications. It has been found that using explicit analytical expressions rather than numerical methods allows for the computation of results in the shortest amount of time with the highest level of accuracy. In second research, he proposed an analytical method based on dynamic stiffness theory for the free vibration analysis of a sandwich beam with three layers. The use of the dynamic stiffness matrix to compute numerical results for a few case studies is discussed. He developed the analytical technique previously utilized for updating the dynamic stiffness matrix in his third research. Shang-Han, Masaya Kurokawa, Nevin Gamze Karsli, et al. [18] used several moulding procedures. When examining the mechanical characteristics of these mixtures using the injection moulding and melt mixing methods, it became clear that the melt mixing approach was more straightforward and cost-effective. Sathujoda et.al [19] observed that the corrosion characteristics, such as the length, depth, and location of the corrosion defect in the shaft, affect variations in the natural and whirl frequencies. Liu, N et.al [20] suggested IGA solid shell element and its performance are checked by using a range of nonlinear shell benchmark problems. Moreover, the impact of the FGM power-law exponent on the shell structures' geometrically nonlinear response is also investigated. Sunil Nayak et.al [21] observed60% reinforced epoxy/basalt fibre composite propeller blade is light weight and effective invention. Murni Awi et.al [22] suggested fibre metal laminates have high amount of potential in the application of aircraft, automobile, medicine, sporting goods, marine. Doo- wan kim [23] converted non graphitizable carbon into graphitizable carbon through breaking- down of boundaries of microdomains using KOH. Sarower Kabir [24] et.al observed hybrid fibre reinforced polymer (HFRP) made up of glass, carbon fibres and epoxy by vacuum infusion moulding technique. It is coated by heat resistant

coating and observed coated HFRP is more efficient. Harini Sosiati [25] et.al observed that the corrosion characteristics, such as the length, depth, and location of the corrosion defect in the shaft, affect variations in the natural and whirl frequencies. Muhammad Hamid Mahmood [26] et.al suggested IGA solid shell element and its performance are checked by using a range of nonlinear shell benchmark problems. Moreover, the impact of the FGM power-law exponent on the shell structures' geometrically nonlinear response is also investigated. The author used a hot compression moulding technique for fabrication with different percentages of fibre loading. With the increase in volume fraction of fibre content, the slight decrease in tensile strength and strain of the composites is seen. Alimin Mahyudin [27] et.al investigated that Activated Carbon Powder (ACP) and Activity Carbon Fiber (ACF) showed hydrophobic behaviour at low relative Pressure Sorbent II (PS II) reduces the desiccant unit size in the DAC system as compared to conventional silica gel under particular conditions. Mr. Dilip S. Choudhari [28] et.al used hand lay-up method for the preparation of composites with different fibre percentages. With the least fibre percentage, highest strength, strain, and modulus of elasticity were obtained. Dilip S. Choudhari [29] et.al prepared different specimens for tensile, flexural, and compression, of carbon fibre reinforced with polyamide 66 composites as per ASTM standards and tested. It is found that all specimens were intact with no delamination issues.

The majority of research studies employed curvature mode, flexibility indices, gradient, and rotations to determine the presence, location, and degree of damage within a structure. Steel structure, frames, reinforced beams, and fibre-reinforced constructions were the primary research topics for these researchers. When it comes to automotive structural components like drive shafts, body frames, and chassis, it is imperative to perform a comprehensive examination of composite materials as soon as damage is detected.

2 Details of Composite Drive Shaft

In the proposed work, the composite drive shaft of a passenger car is analysed. It is a single drive shaft with a circular cross-section of the cantilever which has an outer diameter of 28mm, inner diameter of 22mm and length of 561mm. It is made of Carbon fibre/Polyamide 66 material with bidirectional laminated fibres of higher specific strength than the conventional steel drive shaft. Table 1 lists the mechanical properties of bidirectional Carbon fibre/Polyamide 66 composite materials which are calculated by volume fraction methods, and the actual composite drive shaft is seen in Figure 1.

Fig.1 Composite Drive Shaft

Table 1 Mechanical properties of Carbon fibre reinforced polyamide66

Sr. No.	Properties	Value
1	Density	1800(Kg/m^3)
2	Elastic Modulus in X Direction	230000(MPa)
3	Elastic Modulus in Y Direction	46000(MPa)
4	Elastic Modulus in Z Direction	46000(MPa)
5	Ratio of transverse strain in XY Direction	0.28
6	Ratio of transverse strain in YZ Direction	0.38
7	Ratio of transverse strain in XZ Direction	0.28
8	Modulus of rigidity XY	23000(MPa)
9	Modulus of rigidity YZ	18000(MPa)
10	Modulus of rigidity XZ	23000(MPa)
11	Ultimate tensile strength	4000(MPa)

2.1 Artificial Crack Location

During working condition, the failures of the drive shaft are brought on by a low fatigue cycle, which is due to excessive stress, which weakens certain parts of the shaft and causes early failure. On a healthy drive shaft, an artificial crack is made to identify the existence, location, and extent of fracture. To construct an artificial crack on intact composite drive shaft, finite element analysis is first used to identify the damage-sensitive area. A 92mm distance separates this area from the fixed end. The relation [20] is used to choose the crack dimensions. It is Y= α / β where α =circumferential crack length and β =width in the direction of propagation of crack, and Y=crack ratio (0.4-0.8). Due to the orthotropic behaviour of the composite material by making a crack on the surface that is 1.5 mm long and 1 mm deep, it will be possible to observe how the crack behaves.

The drive shaft put through a predetermined number of fatigue cycles—400, 800, and so forth until the crack appears. At the end, the complete length of crack along the circumference has been developed which is shown in figure 2. Figure 3 represents the experimental set-up for torsional test of composite drive shaft.

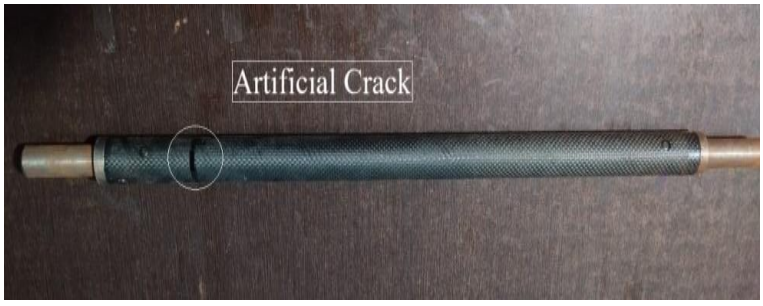

Fig.2 Artificial fracture on the Composite Drive Shaft

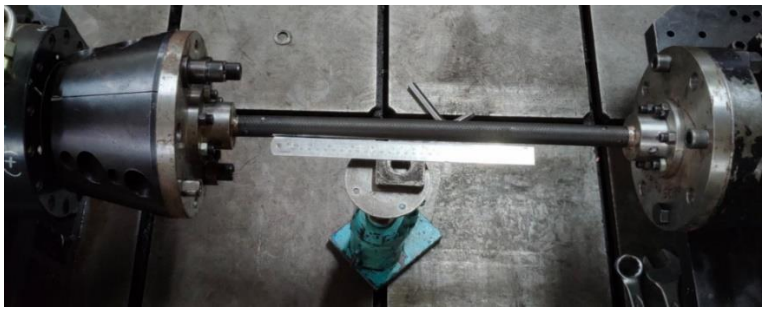

Fig.3 Torsional fatigue test set up of Composite Drive Shaft

2.2 Background

Modal parameters, which are crucial elements of structural dynamics analysis and include characteristic frequency, Eigen modes, flexibility indices, curvatures, and modal rotations, substantially contribute in damage identification. Two of these factors that are used for damage assessment are vibration flexibility and curvature shape. A robust drive shaft is likened to the mathematical fluctuations among the parameters.

2.3 Cantilever Beam Numerical Model

By using CAD-Design, the composite drive shaft is modelled as both intact and damaged cantilever beams, as seen in Figs. 4 and 5. By taking into account equivalent outer and inner diameters and thicknesses (t) along the length of the beam, it has been divided into three equal pieces. In Figures 4 and 5, the digits 1,3,5,7 denote modal displacements, and 2, 4, 6,8,10 denote modal rotations. Only modal rotations are taken into account during the numerical analysis.

Dynamic Equations of a Cantilever Structure is:

$$[M]\left\{\frac{d^2x}{dt^2}\right\} + [C]\left\{\frac{dx}{dt}\right\} + K = 0$$

Drive shafts with and without cracks are modelled using consistent mass. For both healthy and damaged beams, the elemental masses are represented as shown in figure. All dimensions represented are in mm.

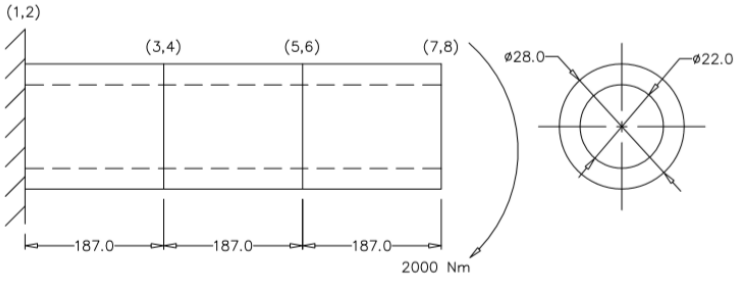

Fig.4 Numerical model of healthy Driveshaft

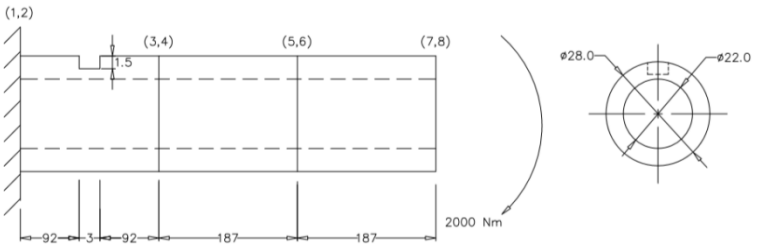

Fig.5 Numerical model of cracked Driveshaft

The Mass matrix for intact and fractured drive shaft is

$$M=\frac{\rho Al}{420}\begin{bmatrix}156 & 22l & 54 & -13l\\ 22l & 4l^2 & 13l & -3l^2\\ 54 & 13l & 156 & -22l\\ -13l & -3l^2 & -22l & 4l^2\end{bmatrix}$$

$$M^*=\frac{\rho Al}{420}\begin{bmatrix}156 & 22l & 54 & -13l\\ 22l & 4l^2 & 13l & -3l^2\\ 54 & 13l & 156 & -22l\\ -13l & -3l^2 & -22l & 4l^2\end{bmatrix}$$

The stiffness for intact and cracked drive shaft is

$$K=\frac{EI}{l^3}\begin{bmatrix}12 & 6l & -12 & 6l\\ 6l & 4l^2 & -6l & 2l^2\\ -12 & -6l & 12 & -6l\\ 6l & 2l^2 & -6l & 4l^2\end{bmatrix}$$

$$K^*=\frac{EI}{l^3}\begin{bmatrix}12 & 6l & -12 & 6l\\ 6l & 4l^2 & -6l & 2l^2\\ -12 & -6l & 12 & -6l\\ 6l & 2l^2 & -6l & 4l^2\end{bmatrix}$$

The characteristic equation for the Eigenvalue calculation for ‘n’ degrees of freedom of intact and fractured composite drive shaft is given by

$$[(K) -\lambda (M)] =0 \text{ and } [(K^*) - \lambda (M^*)] =0$$

The mass matrix normalization of both intact and damaged drive shafts is provided by $[U^T][M][U]$ and$[U^T][M^*][U]$.

3. Analytical Method

The presence, position, and amount of a fracture in a fractured drive shaft are determined using the modal flexibility and modal curvature approaches.

3.1 Modal Flexibility Method

To determine the existence, location, and extent of damage in structures, structural mechanics use this effective modal method. Identifying natural frequencies, mass-normalized mode shape, and the flexibility matrix of structures are also aided by it. For lower modes, it is more accurate, and for higher modes, it converges.

The flexibility matrix of an intact and fractured cantilever drive shaft at a distance x from the fixed end along its length is,

$$[F]_{hx} = \sum_{i=1}^{\infty} \frac{1}{\omega^2} U_x U_x^T$$

$$[F]_{dx} = \sum_{i=1}^{\infty} \frac{1}{\omega^2} U_x U_x^T$$

The change in the flexibility matrix for healthy and cracked drive shaft is,

$$\Delta[F] = [F]_{h\,x} - [F]_{d\,x} = [\sum_{i=1}^{\infty} \frac{1}{\omega^2} U_x U_x^T]_{hx} - [\sum_{i=1}^{\infty} \frac{1}{\omega^2} U_x U_x^T]_{dx}$$

Here, $\omega_i$is the corresponding modal natural frequency. The maximum numerical value of the corresponding element is used to detect the presence and location of fracture.

Below is a step-by-step process for calculating the modal flexibility of both drive shafts.

Assembled Mass and Stiffness Matrix Calculation

For a healthy drive shaft, the stiffness and mass matrices are put together as shown below.

$$K = \begin{bmatrix} 0.184 & 0.046 & 0 \\ 0.046 & 0.184 & 0.046 \\ 0 & 0.046 & 0.092 \end{bmatrix} \times 10^6$$

$$M = \begin{bmatrix} 5.28 & -1.98 & 0 \\ -1.98 & 5.28 & -1.98 \\ 0 & -1.98 & 2.64 \end{bmatrix} \times 10^{-5}$$

For cracked drive shafts, the elemental stiffness and mass matrices are put together as shown below.

$$K^* = \begin{bmatrix} 0.146 & 0.046 & 0 \\ 0.046 & 0.184 & 0.046 \\ 0 & 0.046 & 0.092 \end{bmatrix} \times 10^6$$

$$M^* = \begin{bmatrix} 4.3 & -1.98 & 0 \\ -1.98 & 5.28 & -1.98 \\ 0 & -1.98 & 2.64 \end{bmatrix} \times 10^{-5}$$

3.2 Modal Curvature method

In order to identify damaged components and determine their presence, location, and degree of damage, one mathematical way for doing so is to compare them to undamaged structures. The second-order central difference approach serves as the foundation for the modal curvature. The central difference approach is applied in the modal rotation field to analyse the modal curvatures for both intact and fractured structures. For lower modal frequencies, this technique works better.

One cantilever beam is taken into consideration in this instance with flexural rigidity as EI subjected to curvature K*x for the damaged drive shaft and bending moment Mx and Kx for the healthy drive shaft. Here, ‘x’ represents the distance of corresponding position from the fixed end of the beam and it is given as

$$K_x = \frac{M_x}{EI}$$

$$K^*_x = \frac{M_x}{EI}$$

The local modal curvatures for both intact and fractured drive shafts are obtained using the central difference approximation.

$$K_x = \frac{\psi(j+1)_i - 2\psi(j)_i + \psi(j-1)_i}{l^2}$$

$$K^*_x = \frac{\psi(j+1)_i - 2\psi(j)_i + \psi(j-1)_i}{l^2}$$

The location of damage in the cracked beam is identified by the numerical difference between modal curvatures for both beams.

$$\Delta[K] = [K^*_x] - [K_x] = \left[\frac{\psi(j+1)_i - 2\psi(j)_i + \psi(j-1)_i}{l^2}\right]_{dx} - \left[\frac{\psi(j+1)_i - 2\psi(j)_i + \psi(j-1)_i}{l^2}\right]_{hx}$$

After mass normalization, the position of the crack is located on the modelled healthy and damaged cantilever drive shaft. The healthy beam's mass-normalized eigenvectors are as follows.

$$U_{h1} = \begin{bmatrix} 6.525 \\ -11.30 \\ 13.05 \end{bmatrix} \times 10^{-5} \quad U_{h2} = \begin{bmatrix} -7.92 \\ 0 \\ 7.92 \end{bmatrix} \times 10^{-5} \quad U_{h3} = \begin{bmatrix} 1.385 \\ 2.4 \\ 2.77 \end{bmatrix} \times 10^{-5}$$

The fractured beam's mass-normalized eigenvectors are as follows.

$$U_{d1} = \begin{bmatrix} 1.125 \\ -1.45 \\ 1.57 \end{bmatrix} \times 10^{-4} \quad U_{d2} = \begin{bmatrix} -6.63 \\ -0.811 \\ 6.824 \end{bmatrix} \times 10^{-5} \quad U_{d3} = \begin{bmatrix} 1.16 \\ 2.13 \\ 2.49 \end{bmatrix} \times 10^{-5}$$

Through the use of the central difference approximation, the modal curvature of a healthy and damaged drive shaft for each of the four nodal sites may be determined.

$$K_{h1} = \begin{bmatrix} -0.007 \\ 0.012 \end{bmatrix}, \quad K_{h2} = \begin{bmatrix} 0.00453 \\ 0 \end{bmatrix}, \quad K_{h3} = \begin{bmatrix} -0.0001 \\ -0.0002 \end{bmatrix}$$

$$K_{d1} = \begin{bmatrix} -0.0105 \\ 0.016 \end{bmatrix}, \quad K_{d2} = \begin{bmatrix} 0.0036 \\ -0.0004 \end{bmatrix}, \quad K_{d3} = \begin{bmatrix} -0.00005 \\ -0.00017 \end{bmatrix}$$

For all four modes, the magnitude of modal curvature difference between a intact and fractured beam provides an approximation of the crack's position.

$$\Delta[K]_1 = [K_{d1} - K_{h1}] = \begin{bmatrix} -0.0035 \\ 0.004 \end{bmatrix}$$

$$\Delta[K]_2 = [K_{d2} - K_{h2}] = \begin{bmatrix} -0.00093 \\ -0.0004 \end{bmatrix}$$

$$\Delta[K]_3 = [K_{d3} - K_{h3}] = \begin{bmatrix} 0.00005 \\ 0.00003 \end{bmatrix}$$

For the first three mode forms, the absolute modal curvature differences are denoted as $\Delta[K]_1, \Delta[K]_2, \Delta[K]_3$

Eigenvalue and Eigenvector Calculation Using MATLAB Programming

MATLAB programming is used to calculate the eigenvalues and eigenvectors. The Eigen frequencies for both intact and fractured drive shaft are shown in Table 2.

Table 2 Modal frequencies of intact and fractured drive shaft

Mode No.	Intact drive shaft (Hz)	Fractured drive shaft (Hz)
First	5511	5290
Second	9400	8736
Third	19008	18790

$$[F]_{hx} = \begin{bmatrix} 894.74 & -587.44 & 218.737 \\ -201.91 & 383 & -404.14 \\ 1838.41 & -9882.53 & 16892.49 \end{bmatrix} \times 10^{-20}$$

$$[F]_{dx} = \begin{bmatrix} 1556.8 & -1406.4 & 1216.3 \\ -551.2 & 710.9 & -719.8 \\ 96.6 & -164 & 16720.34 \end{bmatrix} \times 10^{-20}$$

Change in Dynamic Flexibility for intact and fractured Driveshaft's

The change in flexibility between the two drive shafts is shown here.

$$\Delta [\mathrm{F}] = [F]_{dx} - [F]_{hx}$$

$$= \begin{bmatrix} 662.06 & -818.96 & 997.563 \\ -349.29 & 327.9 & -315.66 \\ -1741.81 & 9718.53 & 172.15 \end{bmatrix} \times 10^{-20}$$

The existence and position of fracture are indicated by an increase in flexibility in the relevant element.

4. Results and Discussion

The absolute modal curvature of a healthy and damaged beam can be compared to establish the approximate location of the crack for each of the four modes.

4.1 Presence of Crack

The modal natural frequency is an appropriate metric to validate the existence of cracks on a global scale. Comparisons are performed between the natural frequencies of broken drive shafts and the healthy for lower modes. Natural frequency has been reported to slight decrease for damaged drive shafts. Analytical and experimental approaches were used to determine the frequency variation with mode number for broken and healthy drive shafts, respectively, as shown in Figures 6 and 7. Figure 8 shows frequency change for both the drive shaft.

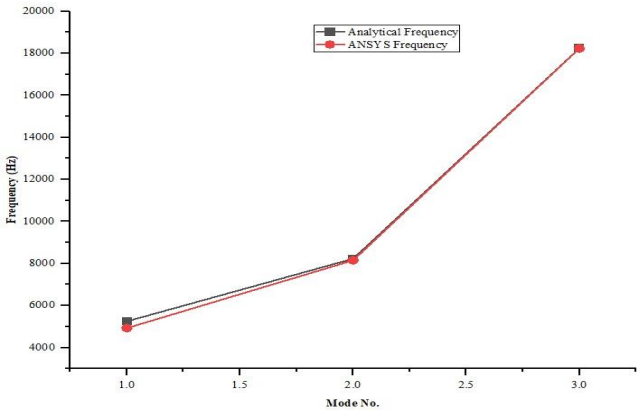

Fig. 6 Healthy drive shaft

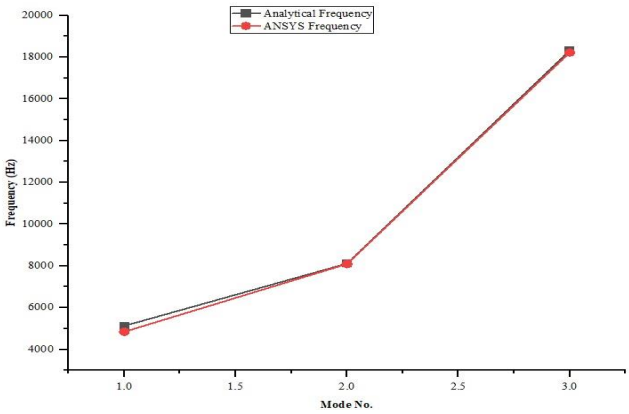

Fig. 7 Cracked drive shaft

4.2 Location of crack

The location of the intentionally created fracture on the composite drive shaft can be determined by applying modal techniques, which take use of the flexibility difference and curvature change properties. The areas of the beam that were 0.187–0.374 m apart showed the largest change in modal flexibility, as seen in Fig. 9. Similar to this, it was found that the modal curvature difference was greatest between the sections of the beam that 0.187-0.374 m, as illustrated in Fig. 9.

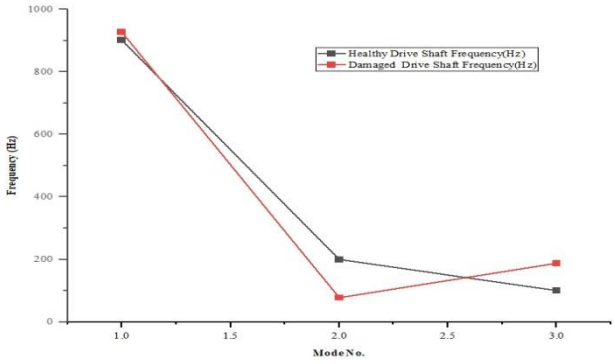

Fig.8 Frequency change among both drive shafts

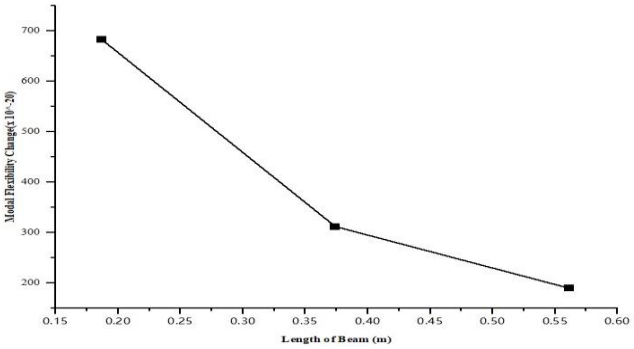

Fig. 9 Flexibility difference between Healthy and Damaged Drive shaft

4.3 Severity of Crack

Modal measures, like modal flexibility and modal curvatures, indicate the severity of a fracture. Fig. 10 indicates that the crack's severity for modal flexibility, it is 60% in fracture zone which is highest in magnitude. In line with this, the modal curvature depiction of the crack severity in Fig. 11 indicates that it is 214.28 and 44.04% for the first and second modes, respectively. Maximum severity is again in fracture zone by modal curvature method.

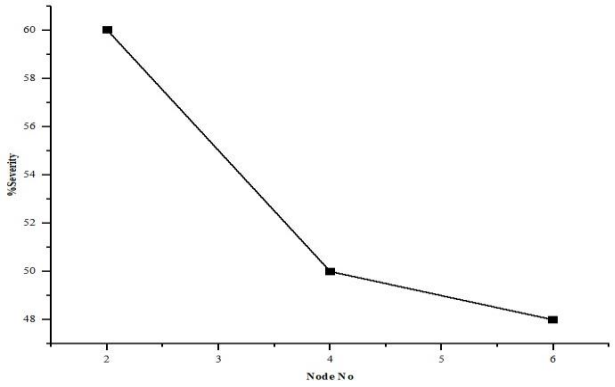

Fig. 10 Modal flexibility method

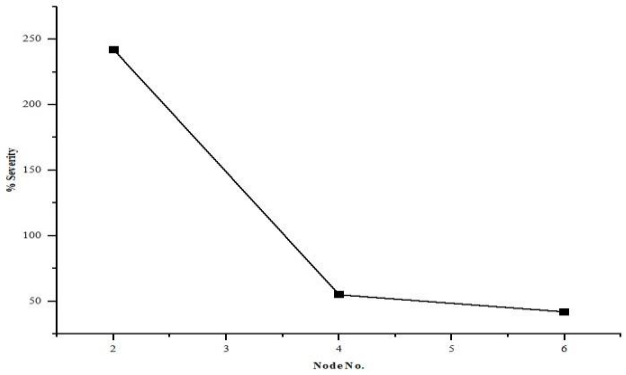

Fig. 11 Modal curvature method

5. Conclusion

Composite drive shaft failure has been analysed using modal flexibility and curvature mode shape techniques. The following conclusion is summarized below:

- Between first and second node there is large variation in natural frequency indicates that there was a fracture in the drive shaft on a global scale at corresponding location.
- By Modal flexibility approach it is observed that the highest modal flexibility shift at the fracture site in the first element, which indicates location of crack.
- Likewise, the identical element's fracture area exhibits a change in modal curvature. Compared to the modal flexibility approach, the fracture is precisely located using the curvature mode shape method.
- Consequently, the position of the fracture is found utilizing two different techniques. Both approaches allowed us to determine the extent of the break between the second and fourth nodal point i.e. in first element. Due to the highest beam amplitude being close to the fracture site, the first mode showed the most severity. The severity at the fracture zone decreases as the amplitude of the mode shape increases with increasing modes.

References

[1] N. I. Jamadar, S. B. Kivade, Rakesh Raushan, “Failure Analysis of Composite Mono Leaf Spring Using Modal Flexibility and Curvature Method” Journal of Failure and prevention, 18 782–790 (2018). doi.org/1.1007/1668-018-0418-4

[2] N. I. Jamadar, S. B. Kivade, Rakesh Raushan “Modal Strain Energy based Crack Inspection in Mono Composite Leaf Spring”, Journal of Failure and prevention, 21 1297-1304 (2021). doi.org/10.1007/s1668-021-01169-49.

[3] V.B. Dawari, G.R. Vesmawala, “Modal Curvature and Fexibility Methods for Honeycomb Damage Identification in Reinforced Concrete Beams”, Elsevier Procedia Engineering, 51 119–124 (2013). doi.org/10.1016/j.proeng.2013.01.018.

[4] A.K. Pandey, M. Biswas, “Experimental verification of flexibility difference method for locating damage in structures”, Journal Sound and Vibration, 184 (2) 311-328 (1995). doi.org/10.1006/jsvi.1995.0319.

[5] E. Reynders, G. De Roeck, “A local flexibility method for vibration- based damage localization and quantification”, Journal of Sound and Vibration, 329 2367–2383 (2010). doi.org/10.1016/j.jsv.2009.04.026.

[6] Zhi-Bo Yang, Maciej Radzienski, Pawel Kudela, Wieslaw Ostachowicz Z. B. Yang, M. Radzienski, P. Kudela, W. Ostachowicz, “Scale-wave number domain filtering method for curvature modal damage detection”, Journal of Composite Structures, 154 396-409 (2016). doi.org/10. 1016/j.compstruct.2016.07.07.

[7] M.M.F. Yuen, “A numerical study of the Eigen parameters of a damaged cantilever”, Journal of Sound Vibration, 103(3) (1985) 301–310. doi.org/10.1016/0022-460X(85)90423-7.

[8] V.S.Bhajantri, S.C.Bajantri, A. M.Shindolkar and S.S. Amarapure, “Design and analysis of composite Drive shaft”, International journal of research in engineering and technology 3(3) 2014 738-745. doi.org/10.1016/j.matpr.2018.01.058.

[9] Dai Gil Lee, Hak Sung Kim, Jong Woon Kim, Jin Kook Kim, “Design and manufacture of an automotive hybrid aluminum/composite drive shaft”, Journal of Composite Structures, 63(1) (2004) 87-99. doi.org/10.1016/S0263-8223(03)00136-3

[10] W. Lestari, P. Qiao, “Damage detection of fiber-reinforced polymer honeycomb sandwich beams”, Journal of Composite Structures, 67(3) (2005) 365–373.doi.org/10.1016/j.composite structure.2004.01.023

[11] H.F.Bauer, “Vibration of a rotating uniform beam”, Journal of sound and vibration. 72(2), (1980) 177-189. doi.org/10.1016/0022-460X (80)90651-3.

[12] Yu. P. Kataev and I.M. Zakirov, “Geometry of hollow polymer-composite shafts for power and torque transmission”, Journal of Russian and Engineering Research 39(1), (2019) 20-21 doi:10.3103/S1068798X19010179.

[13] C. Elanchezhian, Vijaya Ramnath, K.N. Sripada Raghavendra, Mithun Muralidharan, “Design and Comparison of the Strength and Efficiency of Drive Shaft made of Steel and Composite Materials”, Materials Today Proceedings 5(1), (2017) 1000-1007. DOI:10.1016/j.matpr.2017.11.176

[14] P. Satheeshkumar Reddy and Ch. Nagaraju, "weight Optimization and Finite Element Analysis of Composite automotive drive Shaft for maximum Stiffness", Materials Today Proceedings 4(2), (2017) 2390-2396. doi:10.1016/j.matpr.2017.02.088

[15] Banarjee, “Dynamic stiffness formulation and free vibration analysis of centrifugally stiffened Timoshenko beams”, Journal of sound and vibration 247(1), (2001) 97-115. doi.org/10.1006/jsvi.2001.3716.

[16] Banarjee and H. Su, “Development of a dynamic stiffness matrix for free vibration analysis of spinning beams”, Journal of computers and structure 82(23-26), (2004) 2189-2197. doi.org/10.1016/j.compstruc.2004.03.058

[17] Banarjee, A. Ananthapuvirajah and S.O.Papkov, “Dynamic stiffness matrix of a conical bar using the Rayliegh-Love theory with applications”, European Journal of Mechanics / A solids 83 (2020), 1-9.

doi: 10.1016/j.compstruc. 2021.106616.

[18] N.G. Karsli and A. Aytac, “Tensile and Thermo Mechanical properties of short carbon fiber reinforced Polyamide 6 Composites”, Journal of Composites, 51 270–275(2013). doi.org/10.1016/j.compositesb.2013.03.023.

[19] Prabhakar sathujoda, “Effect of Corrosion on the Natural and Whirl Frequencies of a Functionally Graded Rotor-Bearing System Subjected to Thermal Gradients”, Materials, 13(20) (2020) 1-20. doi.org/10.3390/ma13204546

[20] Liu, N. Ren, X.Lua, “An isogeometric continuum Shell element for modeling the nonlinear response of functionally graded material structures”, Journal of Composites structures 237 (2020).

doi.org/10.1016/j.compstruct.2020.111893

[21] Sunil Nayak, M. Prasanna kumar, “Mechanical Characterization and Static Analysis of Natural fiber based composite propeller blade,” EVERGREEN Joint Journal of Novel Carbon Resource Sciences & Green Asia Strategy, 10 (02) 805-812 (2023).

https://www.tj.kyushu-u.ac.jp/evergreen/contents/EG2023-10_2_content/pdf/p805-812.pdf

[22] Murni Awi, Ahmad Sufiyan Abdullah, “A review on mechanical properties and response of fiber metal laminate under impact loading (Experiment),” EVERGREEN Joint Journal of Novel Carbon Resource Sciences & Green Asia Strategy, 10(01) 111-129 (2023).

https://www.tj.kyushu-u.ac.jp/evergreen/contents/EG2023-10_1_content/pdf/p111-129.pdf

[23] Doo- wan kim, Hyun-sig kil, Koji Nakabayashi, seong-Ho Yoon, "Improvement of electric conductivity of non-graphitizable carbon material via breaking-down and merging of the microdomains," EVERGREEN Joint Journal of Novel Carbon Resource Sciences & Green Asia Strategy, 04 (01) 16-20 (2017).

https://carbon.cm.kyushu-u.ac.jp/publication/index-en.htm

[24] Sarower Kabir, Faiz Ahmad, Khurshid malik, Norlin nosbi, Laurent Guillaumat, "Effect of heat resistant coating on the drilled hole quality of hybrid fiber reinforced epoxy composite," EVERGREEN Joint Journal of Novel Carbon Resource Sciences & Green Asia Strategy, 07 (04) 530-537 (2020). DOI:10.5109/4150472

DOI:10.5109/1657738

[25] Harini Sosiati, Yankeisna Auda Shofie, Aris Widyo Nugroho, "Tensile Properties of Kenaf/E-glass Reinforced Hybrid Polypropylene (PP) Composites with Different Fiber Loading," EVERGREEN Joint Journal of Novel Carbon Resource Sciences & Green Asia Strategy, 05 (02) 1-5 (2018).

doi.org/10.5109/1936210.

[26] Muhammad Hamid Mahmood, Muhammad Sutan, Takahiko Miyazaki, "Study on Water-Vapor Adsorption onto Polymer and Carbon-Based Adsorbents for Air-Conditioning Applications," EVERGREEN Joint Journal of Novel Carbon Resource Sciences & Green Asia Strategy, 06 (03) 32-36 (2019).

doi.hdl.handle.net/2324/2349297.

[27] Alimin Mahyudin, Syukri Arief, Hairul Abral, Emriadi, Mulda Muldarisnur, Mila Puteri Artik, "A Mechanical Properties and Biodegradability of Areca Nut Fiber-reinforced Polymer Blend Composites," EVERGREEN Joint Journal of Novel Carbon Resource Sciences & Green Asia Strategy, 07 (03) 366-372 (2020).

http://hdl.handle.net/2324/4068618.

[28] Mr. Dilip S. Choudhari1, Dr. Vyasraj J. Kakhandki, "Characterization and Analysis of Mechanical Properties of Short Carbon Fiber Reinforced Polyamide66 Composites" EVERGREEN Joint Journal of Novel Carbon Resource Sciences and Green Asia Strategy, 08 (04), 768-776, (2021).

https://doi.org/10.5109/4742120

[29] Dilip S. Choudhari, Dr. Vyasraj J. Kakhandki, "Comprehensive study and analysis of mechanical properties of chopped carbon fibre reinforced nylon 66 composite materials," Materials Today: Proceedings Elsevier 44 4596-4601(2021). doi.org/10.1016/j.matpr.2020.10.828